A Return Stroke NO_x Production Model

WILLIAM J. KOSHAK

NASA Marshall Space Flight Center, Huntsville, Alabama

RICHARD J. SOLAKIEWICZ

Chicago State University, Chicago, Illinois

HAROLD S. PETERSON

Universities Space Research Association, Huntsville, Alabama

(Manuscript received 30 April 2014, in final form 18 September 2014)

ABSTRACT

A model is introduced for estimating the nitrogen oxides ($NO_x = NO + NO_2$) production from a lightning return stroke channel. A realistic modified transmission line model return stroke current is assumed to propagate vertically upward along a stepped leader channel of 0.1-cm radius. With additional assumptions about the initial radial expansion rate of the channel, the full nonlinear differential equation for the return stroke channel radius $r(z, t)$ is solved numerically using Mathematica V9.0.1.0. Channel conductivity and channel air density are adjustable constants, and the model employs typical atmospheric profiles of temperature, pressure, and density. The channel pressure is modeled by a dynamic pressure expression. Channel temperature is extracted from the pressure by a minimization technique that involves a generalized gas law appropriate for high temperatures where dissociation and ionization are important. The altitude and time variations of the channel energy density are also obtained. Three model runs, each with different input parameters, are completed. Channel radii at sea level range from about 1.7 to 6.0 cm depending on the model inputs and are in good agreement with other investigators. The NO_x production from each 1-m segment of the channel is computed using conservation of energy and equilibrium freeze-out-temperature chemistry. Because the NO_x per meter of channel is computed as a function of altitude, extensions of the results to tortuous and branched channels are possible and lead to preliminary estimates of total return stroke NO_x. These estimates are found to be smaller than the return stroke NO_x values obtained from the NASA Lightning Nitrogen Oxides Model (LNOM).

1. Introduction

Several gas dynamic models have been developed to analyze explosions in air. For example, Taylor (1950) developed a model for spherical blast waves that can be applied to thermonuclear explosions. For cylindrically symmetric explosions, Drabkina (1951) described the rapid shockwave radial expansion of a spark channel. Lin (1954) formally extended the analysis of Taylor (1950) to a cylindrical geometry, with applications for characterizing meteor and hypersonic missile trails, spark channels, and lightning discharges.

Additional notable efforts in gas dynamic modeling include the work of Sakurai (1954) and the strong shock approximation of Braginskii (1958). The work of Braginskii has gained attention in both engineering and scientific applications [e.g., resistance and inductance of gas arcs (Barannik et al. 1975), lightning return stroke channel resistance (DeConti et al. 2008; DeConti and Visacro 2009), and lightning nitrogen oxides (LNO_x) production (Cooray et al. 2009)].

More elaborate gas dynamic models were subsequently developed. For example, a model that is applicable across both strong and weak shock domains and that employed an equation of state for air at high temperature was introduced (Plooster 1968, 1970) and then directly applied to lightning return strokes (Plooster 1971). In addition, a detailed gas dynamic model introduced by Paxton et al. (1986) included energy loss in the return stroke channel due to radiation.

Corresponding author address: William Koshak, Earth Science Office, Mail Stop ZP11, NASA Marshall Space Flight Center, 320 Sparkman Drive, Huntsville, AL 35805.
E-mail: william.koshak@nasa.gov

DOI: 10.1175/JAS-D-14-0121.1

The motivation for the present work is multifaceted. First, LNO_x indirectly influences our climate since it plays a role in controlling the concentration of ozone (O_3) and hydroxyl radicals (OH) in the atmosphere (Huntrieser et al. 1998); O_3 is a greenhouse gas that affects the radiative balance of the Earth–atmosphere system, and OH affects the concentration of several other greenhouse gases. In addition, LNO_x is the most important source of NO_x in the upper troposphere (Schumann and Huntrieser 2007; Zhang et al. 2003). Therefore, improving the modeling of LNO_x production is highly desired and is a central focus of our study. Second, we wanted to develop a reasonably rigorous model for return stroke NO_x production that could be used for independent comparison with, and validation of, the empirically based return stroke NO_x production model employed in the National Aeronautics and Space Administration (NASA) Lightning Nitrogen Oxides Model (LNOM; Koshak et al. 2009, 2010; Koshak and Peterson 2011; Koshak et al. 2014). LNOM makes estimates of NO_x production from the many different discharge processes in a lightning flash (including the return stroke in a ground flash) in order to obtain an estimate of the total NO_x produced by the flash. Third, we wanted it to be possible, as well as practical, to replace LNOM's empirically based return stroke NO_x parameterization with the rigorous model developed here. The ability to "plug and play" the return stroke NO_x production module in LNOM greatly facilitates optimizing the testing and accuracy of the LNOM. Fourth, since there are uncertainties in key chemical NO_x sinks that affect top-down estimates of NO_x (Stavrakou et al. 2013), there is a desire to improve bottom-up estimation such as provided by our model. Finally, there is a general desire to continuously improve the accuracy of LNOM in preparation for its application to future satellite lightning data. The Geostationary Operational Environmental Satellite R-series (GOES-R) is due to launch in early 2016 as of this writing and will include the Geostationary Lightning Mapper (GLM; Goodman et al. 2013). The GLM will map the locations and time of occurrence of total (ground flash and cloud flash) lightning activity continuously day and night with near-uniform storm-scale spatial resolution and with a product refresh rate of under 20 s over the Americas and adjacent oceanic regions. Fully optimizing the accuracy of LNOM is desired to ensure reasonable assignments of LNO_x production to GLM ground and cloud flashes. This, in turn, facilitates global climate–chemistry and regional air quality modeling efforts that depend on accurate LNO_x parameterizations and LNO_x emission inventories.

Section 2 introduces the model and describes how numerical solutions for various channel properties are obtained. What fundamentally sets our gas dynamic model apart from others is that it completes the extra steps required to estimate return stroke NO_x production. This means that the model obtains solutions for several channel properties (i.e., radius, expansion rate, pressure, temperature, and energy density) not only as a function of time, but also as a function of altitude and the detailed characteristics of the return stroke current. Section 3 provides results of some basic model runs and intercompares these results with other investigators. Results for return stroke NO_x production are also compared with the empirical-based results derived from LNOM. Section 4 summarizes the effort.

2. Model description

As an overview, note that the model begins with an idealized vertically oriented stepped leader channel of fixed cross-sectional radius and a length extending from sea level to an altitude of 6.5 km. The value of 6.5 km is a reasonable height of the negative charge layer in a thundercloud (Koshak and Krider 1989). The channel is embedded in a realistic atmospheric environment with specified temperature, pressure, and density profiles. Next, a return stroke current propagates up the stepped leader channel, thereby heating and rapidly expanding the channel radius as a function of altitude and time. Likewise, the return stroke channel pressure, temperature, and energy density all rapidly increase. The decay of the return stroke current and the cooling of the channel due to radial channel expansion eventually reduce the channel radial expansion rate. This, in turn, results in a reduction in channel pressure, temperature, and energy density. Because the channel radial expansion rate subsides and the channel pressure approaches the ambient atmospheric pressure, the model channel radius attains an altitude-dependent maximum value.

The following subsections provide details on each of the key components of the return stroke NO_x production model.

a. Ambient atmosphere

The environmental profiles of atmospheric temperature $T_e(z)$ and pressure $p_e(z)$ employed in the model are given by the reference state of the Fifth-Generation Pennsylvania State University–National Center for Atmospheric Research (NCAR) Mesoscale Model (MM5) as discussed in Archer (2004):

$$T_e(z) = \left[T_e^2(0) - \frac{2gAz}{R_d}\right]^{1/2} \quad \text{and} \tag{1}$$

$$p_e(z) = p_e(0)\exp\left\{-\frac{T_e(0)}{A} + \left[\frac{T_e^2(0)}{A^2} - \frac{2gz}{AR_d}\right]^{1/2}\right\}. \tag{2}$$

Here, g is the acceleration of gravity, R_d is dry-air gas constant, $T_e(0)$ is sea level temperature (taken as approximately 298.1 K in our model runs), $p_e(0)$ is the sea level pressure and equal to 101 325 Pa, and $A = 50$ K is the temperature difference across one e folding of the pressure.

The vertical profile of air density is given by the ideal gas law

$$\rho_e(z) = \frac{p_e(z)}{R_d T_e(z)}. \tag{3}$$

b. Channel current

In the model of Braginskii (1958), it had to be assumed that the current source was a linear function of time, but this is not adequate for purposes of return stroke modeling. Similarly, Plooster (1971) and Paxton et al. (1986) both avoided the use of an optimal return stroke current model in favor of a more simplified current source that had a linear rise to peak followed by an exponential decay.

In our model, a realistic return stroke current source is employed. It is called the modified transmission line model (MTLM) introduced by Heidler (1987). With the return stroke current front propagating vertically up the stepped leader channel with speed w, the current at altitude $z \leq wt$ in the MTLM in terms of a shifted time coordinate $t' = t - z/w$ is

$$i(z,t) = \left\{ \frac{I_{o1}(t'/\tau_1)^2 e^{-t'/\tau_2}}{\eta[(t'/\tau_1)^2 + 1]} + I_{o2}(e^{-t'/\tau_3} - e^{-t'/\tau_4}) \right\} e^{-z/\lambda}. \tag{4}$$

The value of the current is zero when the front has not yet reached the altitude considered (i.e., when $z > wt$). The MTLM is commonly used to model return stroke radiated fields [see the discussion by Nucci et al. (1990) for additional details]. The values of the constants are $\eta = 0.845$, $I_{01} = 9900$ A, $I_{02} = 7500$ A, $\tau_1 = 0.072\,\mu$s, $\tau_2 = 5.0\,\mu$s, $\tau_3 = 100.0\,\mu$s, and $\tau_4 = 6.0\,\mu$s. Note here that time t is in microseconds, and altitude z is in meters. In addition, we assume that $w = 1.3 \times 10^8\,\mathrm{m\,s^{-1}}$ and $\lambda = 1750$ m, which are both in accordance with the ranges given in Nucci and Rachidi (1989).

c. Fundamental equations

The primary equations of the gas dynamic model are

$$p = \rho R_d T G(\rho, T) - p_m, \tag{5}$$

$$\epsilon = \rho R_d T F(\rho, T), \quad \text{and} \tag{6}$$

$$i^2 R - L = \frac{d(\epsilon V)}{dt} + p\frac{dV}{dt}. \tag{7}$$

The dependent variables $p = p(z,t)$, $\rho = \rho(z,t)$, $T = T(z,t)$, and $\epsilon = \epsilon(z, t)$ are the return stroke channel pressure (Pa), channel air density ($\mathrm{kg\,m^{-3}}$), channel temperature (K), and channel energy density ($\mathrm{J\,m^{-3}}$), respectively. The return stroke current is $i = i(z,t)$, as modeled in (4). Equations (5) and (6) were essentially introduced in Plooster (1968), but we have added an extra pressure term ($-p_m$) into (5) to acknowledge the presence of a self-magnetic pinch produced by the return stroke current. The magnetic pinch exerts an inward radial pressure counter to the first term (which is a thermal pressure). Equations (5) and (6) are for a mixture of diatomic nitrogen and diatomic oxygen that Plooster calls "Air2" and that closely resembles actual air; that is, trace gases are neglected. The rather complicated functions G and F are implicitly provided and discussed in Plooster (1968) so are not repeated here. These functions account for the effects of dissociation and ionization that occur at high temperatures (i.e., $T \gtrsim 10\,000$ K). Additional discussion of the remaining variables and the physical interpretation of Eqs. (5)–(7) follow.

Equation (5) is a generalized gas law, or magnetothermal equation of state, that holds at the high temperatures of the return stroke channel. It reduces to the ideal gas law if the temperature is sufficiently low (such that $G \sim 1$) and the current is sufficiently low (such that p_m can be neglected).

Equation (6) is the associated generalized caloric equation of state. We have weighted our caloric equation of state by a factor of ρ and have made a minor notational change relative to what was provided in Plooster (1968). The weighting by ρ has the advantage that the form of (6) is identical to the form of (5) when $p_m = 0$.

Equation (7) is an expression of the time rate of change of the first law of thermodynamics (i.e., $dQ/dt = dU/dt + pdV/dt$) applied to a cylindrical segment of the channel. The net energy input into the channel segment is $dQ/dt = i^2R - L$, where i^2R is the familiar joule heating supplied by the return stroke current, R the electrical resistance of the channel segment, and L represents any energy loss mechanisms. The term $dU/dt = d(\epsilon V)/dt$ is the rate of change of stored internal energy of the channel segment, and pdV/dt is the work that the channel segment does on the environment. Note that the channel segment is a vertical cylindrical channel element of volume $V = \pi r^2 l$, where r is the cross-sectional channel radius and $l = 1$ m is the vertical thickness of the cylindrical element.

d. Simplifying assumptions

First, we assume fixed values for certain return stroke properties. Specifically, the return stroke air density $\rho = \rho_{\mathrm{rs}} = 0.0135\,\mathrm{kg\,m^{-3}}$ is assumed and is based on the typical values obtained in the spectroscopic observations and

modeling of Orville (1968a). The return stroke channel conductivity σ (see later) is assumed to be $2.2 \times 10^4\,\mathrm{S\,m^{-1}}$ (DeConti et al. 2008).

Second, we have neglected the self-magnetic pinch effect imposed by the return stroke current; that is, we set $p_m = 0$. The inward radial pressure gradient is given by $\mathbf{J} \times \mathbf{B}$, where $\mathbf{J}$ is the return stroke current density and $\mathbf{B}$ is the magnetostatic induction produced by the return stroke current at a particular moment in time. Since the inward radial magnetic pinch inhibits channel expansion, neglecting this effect leads to overestimating maximum channel radius. Moreover, it will be advantageous to express the channel pressure in terms of the familiar dynamic pressure $K\rho_e(z)v^2$, where v is the radial expansion rate of the channel (i.e., the time derivative of the channel radius) and K is the coefficient of resistance. This gives

$$p = p_e(z) + K\rho_e(z)v^2. \tag{8}$$

Even though we employ this expression for pressure, we still require that it equals the value of p given in (5) for a given channel temperature (where again $p_m = 0$). Equation (8) follows a similar approximation made in Braginskii (1958) for a channel element at sea level. However, we have generalized Braginskii's expression for any channel altitude, and we have also added an ambient pressure term $p_e(z)$. Without this added term, p would be zero when the channel stops growing (i.e., when $v = 0$), which is absurd. Since the channel pressure never reaches zero, the value of v would always be positive implying that the radius grows without bound (also absurd). Hence, Braginskii's channel radius grows without bound since ambient pressure was neglected. Since we use a nonzero value of $p_e(z)$ as given in (2), our maximum channel radius is achieved when p falls to the ambient level $p_e(z)$ such that $v = 0$.

Third, we follow a simplifying assumption made in Braginskii (1958) regarding energy density but again make some improvements on the assumption. The ideal gas law gives $p = \rho R_d T = \rho(c_p - c_v)T = \rho(\gamma - 1)u = (\gamma - 1)\epsilon$. Hence, the Braginskii approximation for channel energy density is $\epsilon = p/(\gamma - 1)$ with $\gamma = 1.22$. Here, c_p and c_v are the specific heats at constant pressure and constant volume, respectively, $\gamma = c_p/c_v$, and the specific internal energy is $u = c_v T$. Instead of working with an ideal gas, we combine (5) and (6) and the assumption $p_m = 0$ to obtain

$$\epsilon = \frac{p}{\Gamma - 1}, \tag{9}$$

where $\Gamma = 1 + G/F = 1 + (\gamma - 1)G$. That is, Γ represents a generalized form of γ since it is valid across a larger temperature range. Note that our expression for energy density reduces to Braginskii's when the channel temperature is sufficiently low (i.e., when $G \sim 1$). Using the functions G and F provided in Plooster (1968), we generated a plot of the temperature dependence of $\Gamma(\rho_{rs}, T)$ as shown in Fig. 1. In the temperature range of importance in this work (i.e., $T = 10\,000$–$30\,000$ K) the mean value (standard deviation) of $\Gamma(\rho_{rs}, T)$ is 1.155 03 (0.015 58) or a ratio of standard deviation to mean of only 1.3%. Given this weak temperature dependence, we can safely apply the expression in (9) with Γ taken as constant. In practice, our model employs a (perhaps slightly more accurate) value for this constant of $\Gamma \sim 1.14$ given in Fig. 2.4 of Bauer (1990). In any case, note that our values of Γ of 1.155 or 1.14 are considered an improvement over Braginskii's value of 1.22. Again, since $\Gamma = 1 + (\gamma - 1)G$, $\Gamma = \gamma$ only when the channel temperature is sufficiently low.

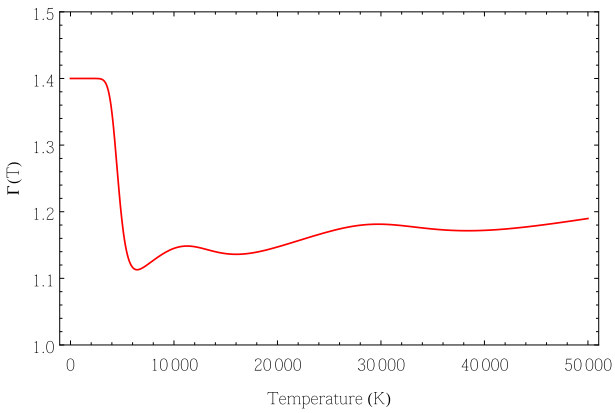

FIG. 1. Variation of Γ with temperature when $\rho = \rho_{rs}$.

Fourth, following the work of Drabkina (1951) and Braginskii (1958), we assume that the coefficient of resistance is $K = 2/(\Gamma + 1)$, which for our value of $\Gamma = 1.14$ gives a value of $K \sim 0.935$.

Finally, we neglect all other possible forms of energy loss from the channel; that is, we assume $L = 0$. In other words, apart from cooling due to channel expansion, we neglect all other cooling mechanisms. Some of these mechanisms have been examined by other investigators: thermal conduction (Braginskii 1958), turbulent mixing (Picone et al. 1981), and radiation (Paxton et al. 1986). However, there is still debate in the literature as to which of these cooling mechanisms are most important (e.g., Hill 1987; Paxton et al. 1987). These ancillary cooling mechanisms represent a loss of energy to the return stroke channel, so neglecting these mechanisms leads to overestimating the maximum channel radius attained.

e. Channel radius and radial velocity

From elementary physics, the channel segment resistance R is the channel resistivity (i.e., inverse conductivity σ) times the channel segment length l divided

by the channel segment cross-sectional area πr^2. Therefore, joule heating can be expressed as $i^2R = i^2l/(\sigma\pi r^2)$. The rate of change of the internal energy is simply $d(\epsilon V)/dt = [1/(\Gamma - 1)]d(p\pi r^2 l)/dt$, where we have used (9) and the definition of the cylindrical volume segment. Finally, the work term is $pdV/dt = pd(\pi r^2 l)/dt$. Substituting these three expressions into (7), using (8), and maintaining the assumptions that $p_m = 0$ and $L = 0$ gives

$$r^4\frac{dr}{dt}\frac{d^2r}{dt^2} + \Gamma r^3\left(\frac{dr}{dt}\right)^3 + \phi r^3\frac{dr}{dt}p_e = \psi i^2 \qquad (10)$$

with the coefficients

$$\phi = \frac{\Gamma}{K\rho_e}, \quad \psi = \frac{\Gamma - 1}{2\pi^2 K\rho_e\sigma}. \qquad (11)$$

The reader should keep in mind which variables have altitude and time dependence; that is, $r = r(z, t)$, $i = i(z, t)$, $p_e = p_e(z)$, $\rho_e = \rho_e(z)$, $\phi = \phi(z)$, and $\psi = \psi(z)$.

In addition, the channel expansion rate (i.e., radial velocity of the channel) is simply the derivative of the channel radius

$$v = v(z, t) = \frac{dr}{dt}. \qquad (12)$$

In practice, one solves (10) numerically for the channel radius given appropriate initial conditions, and then a numerical derivative of the solution is taken to obtain the radial velocity. Details of the solution process are provided in the next subsection.

f. Numerical solution

Equation (10) is a first-degree, second-order, nonlinear ordinary differential equation (ODE) for the radius as a function of time, with the altitude viewed as a parameter. The ODE is amenable to numerical solution at a given value of z using the ParametricNDSolve utility of Mathematica V9.0.1.0. But, this requires the initial conditions for the channel radius and radial expansion rate.

Since the return stroke current takes time to propagate up the stepped leader channel, we replace $i(z, t)$ on the RHS of (10) with the current source $j(z, t') = i(z, t - z/w)$ and solve each ODE for z with respect to the shifted time $t' = t - z/w$. In this shifted time coordinate, $t' = 0$ always corresponds to the moment the return stroke current front arrives at z, no matter what channel altitude one considers.

For the initial channel radius, we assume that $r(z, z/w) = r(z, t' = 0) = 0.1$ cm (DeConti et al. 2008).

The initial radial velocity is more difficult to estimate than initial channel radius. For perspective, the study of laboratory spark discharges by Abramson et al. (1947) using a mirror scanning technique suggested a radial expansion rate of laboratory spark discharges of 1–5 km s^{-1}. In addition, the radial solution given in Fig. 4 of Plooster (1971) has an initial radial velocity of about 1.17 km s^{-1}.

Since the return stroke current in (4) at z is zero at the moment that the return stroke current front arrives at z [i.e., $i(z, z/w) = 0$], the return stroke current itself initially provides no joule heating (and hence channel radial expansion) at the arrival time $t = z/w$. Therefore, the initial radial expansion of the channel is assumed to be solely due to the thermal pressure of the stepped leader. From Orville (1968b), the stepped leader temperature prior to the return stroke is approximately $T_s = 10\,000$ K. Hence, applying (5) and (8) to the stepped leader and again assuming $p_m = 0$, we can equate the stepped leader thermal pressure $p_s = \rho_s R_d T_s G(\rho_s, T_s)$ to the expression $p_e(z) + K\rho_e(z)v^2(z, z/w)$ to estimate the initial condition for the radial velocity as

$$v(z, t' = 0) = \sqrt{\frac{\rho_s R_d T_s G(\rho_s, T_s) - p_e(z)}{K\rho_e(z)}}. \qquad (13)$$

When applying (13), the value of the stepped leader air density is assumed to be $\rho_s \sim 10\rho_{rs}$. This results in a radial velocity of about 0.78 km s^{-1} at sea level, which is reasonably close to the results of Abramson et al. (1947) and Plooster (1971). We do not assume a smaller value of ρ_s because this would result in adversely lowering the initial radial velocity even farther below the 1 km s^{-1} level.

In any case, we do not rigidly adhere to the estimate in (13) but only propose it as a potential estimate given the lack of direct observations of the stepped leader radial expansion. Certainly, one could consider using (as we do in section 3) a larger initial radial velocity to examine the impact on the channel radius solutions.

g. Channel pressure, energy density, and temperature

Obtaining the channel pressure and energy density is straightforward. The channel pressure is obtained by computing the radial velocity from (12) and then applying (8). The energy density is then computed from the channel pressure using (9).

To obtain the channel temperature requires more effort. We apply Mathematica's NDMinimize utility to find the temperature that minimizes the following scalar function:

$$S(T) = \{\rho_{rs} R_d T G(\rho_{rs}, T) - [p_e(z) + K\rho_e(z)v^2]\}^2. \qquad (14)$$

That is, we find the temperature the channel would need to be such that the generalized gas law pressure (with $p_m = 0$) is equivalent to the channel pressure given in (8). Since we fix the return stroke air density (i.e.,

$\rho = \rho_{rs} = 0.0135\,\mathrm{kg\,m^{-3}}$), temperatures derived from (14) are valid only for those times when the channel temperature is high such that this assumed fixed air density value approximately holds. For example, long after the channel stops expanding ($v = 0$) the channel approaches ambient pressure and temperature and the fixed value for ρ_{rs} is no longer appropriate. This means that (14) overestimates the temperature as soon as the true return stroke channel air density begins increasing above our fixed estimate.

h. Return stroke NO_x production profiles

To estimate NO_x production from each return stroke channel segment, we follow the methodology outlined in the derivation of (5) in Cooray et al. (2009) but explicitly emphasize the altitude dependence. As the channel segment centered at z cools because of its radial expansion, the channel pressure eventually subsides to the ambient pressure. At this moment t_m, the channel stops expanding and it reaches its maximum radius; that is, $r_m = r(z, t = t_m)$. [Note here that we are expressing time in terms of the absolute time coordinate t, not the shifted time coordinate t' utilized just for solving (10).] The channel temperature and energy density at the instant the channel acquires its maximum radius is given by $T_m = T(z, t = t_m)$ and $\epsilon_m = \epsilon(z, t = t_m)$. The channel further cools to the freeze-out temperature $T_f = 2660\,\mathrm{K}$ (Cooray et al. 2009; Zeldovich and Raizer 2002), due to turbulent mixing, radiation, and conduction, and is still at the ambient pressure. At T_f, the ideal gas law is obeyed; that is, $G(\rho_{rs}, T_f) = 1$, so the number of gas molecules in the channel segment is simply $N_f = [p_e(z)V_f]/(kT_f)$, where V_f is the channel segment volume at the freeze-out temperature and k is the Boltzmann constant. However, by the conservation of energy, we have $\epsilon_f V_f = \epsilon_m V_m$. Using this last expression to represent V_f, using the form in (9) to express the energy densities, and noting that $V_m = \pi r_m^2 l$, one can obtain the NO_x production $P(z) = f^o N_f$ from the channel segment at z as

$$P(z) = f^o \frac{p_e(z)}{kT_f}\left(\frac{\Gamma_f - 1}{\Gamma - 1}\right)\pi r_m^2(z) l. \qquad (15)$$

Here, $f^o \sim 0.029$ is the nitric oxide (NO) equilibrium mixing ratio (Borucki and Chameides 1984; Chameides 1986), which is the fraction of NO molecules in the gas at temperature T_f; it is understood that most of the NO_x ($=NO + NO_2$) produced by the discharge is in the form of NO (Wang et al. 1998). Since we find from our model runs (section 3) that $6000 \lesssim T_m \lesssim 12\,000\,\mathrm{K}$, we make the reasonable assumption that $\Gamma(\rho_{rs}, T_m) \sim \Gamma = 1.14$. In addition, $\Gamma_f \sim 1.2894$ as given in Keenan et al. (1983).

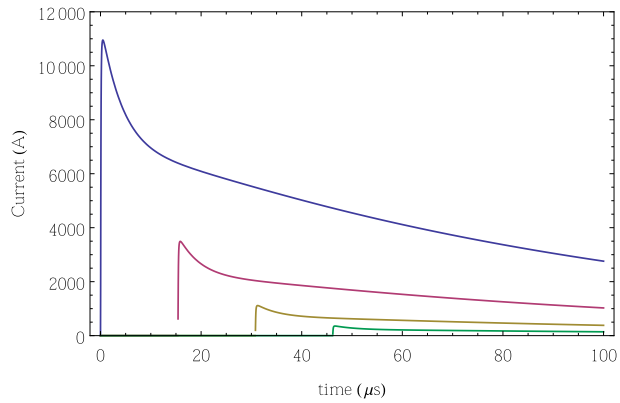

FIG. 2. Current used for model run 1 for different altitudes: 0 (blue curve), 2 (red curve), 4 (yellow curve), and 6 km (green curve). The current waveform parameters are described in section 2b.

3. Results and discussion

In this section we provide a baseline model run that employs a baseline return stroke current and a baseline initial radial velocity profile. To illustrate how model results change with different input parameters, we provide two additional model runs: one with a larger initial radial velocity profile than the baseline and one with a larger return stroke peak current than the baseline. The initial condition on the channel radius remains fixed at 0.1 cm for all the runs below.

a. Model run 1 (baseline)

In this model run, the return stroke current described in section 2b is used; a plot of the time variation of the current for several altitudes is given in Fig. 2. Note that the peak current at the ground is just under 11 kA. About 50% of negative polarity ground flashes have peak currents that exceed 30 kA (Rakov and Uman 2003), so 11 kA is a smaller than typical event. The initial radial velocity profile is given by (13) and is plotted in Fig. 3. Figures 4–8 provide the numerical solution results for the channel radius, radial velocity, pressure, energy density, and temperature, respectively. The channel radius results in Fig. 4 are fundamental since all the other channel attributes are derived from these curves.

The radii for $z = 0$ (blue curve) are in good agreement with the plots of radius versus time provided in Fig. 4 of Plooster (1971), which had a channel radius of about 1.5 cm at 35 μs. The radii results, and those to follow, are also in good agreement with the 1–4-cm range suggested by Oetzel (1968). In addition, for the peak current of just under 11 kA employed in this model run, our maximum radii ($z = 0$) also match up well with the value given in Fig. 1 of Cooray et al. (2009).

Note from Fig. 6 for $z = 0$ km (blue curve) that the channel pressure approaches the ambient atmospheric

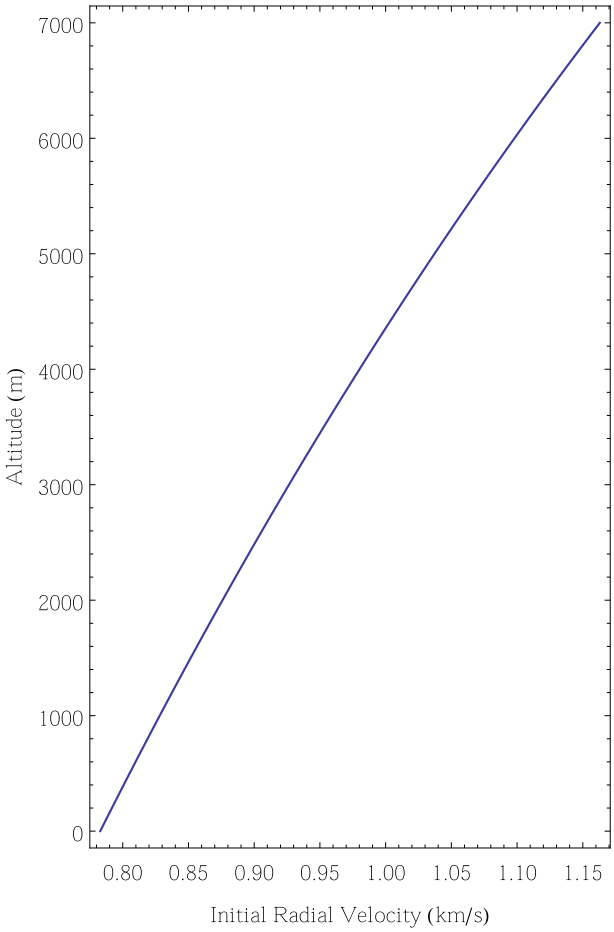

FIG. 3. Initial condition for the channel radial velocity for model run 1.

pressure in about 20–30 μs, which is in good agreement with the spectroscopic observations and modeling provided in Fig. 3 of Orville (1968a). In this same time interval, the channel radius begins to level off, and the channel radial velocity subsides.

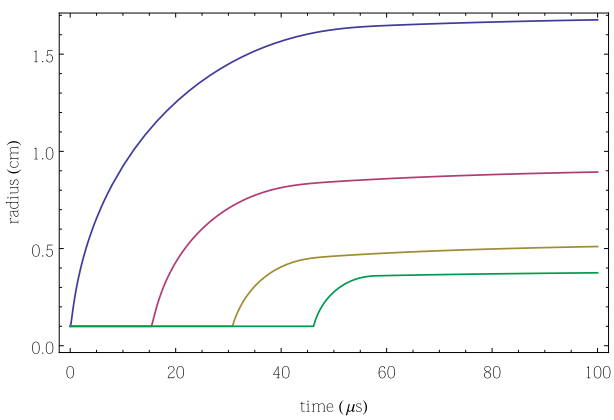

FIG. 4. Channel radius vs time for various altitudes (model run 1). See Fig. 2 caption for altitude curve color key.

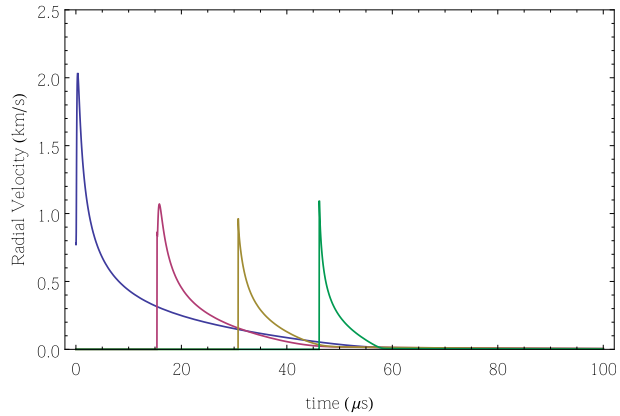

FIG. 5. Channel radial velocity vs time for various altitudes (model run 1). See Fig. 2 caption for altitude curve color key.

The energy density values shown in Fig. 7 are on the order of several megajoules per cubic meter (i.e., several joules per cubic centimeter) and hence are in basic agreement with the 1 J cm^{-3} requirement specified in Picone et al. (1981) for creating a hot channel at sea level pressure.

Finally, the channel temperature (Fig. 8 for $z = 0$, blue curve) is in reasonable agreement with the spectroscopic study by Orville (1968a). To save on CPU time in the minimization of (14) and to physically constrain the peak temperature to a reasonable value, we have placed an artificial cap on the peak temperature of 30 000 K. In addition, note that all the channel temperature curves in Fig. 8 decay to artificially high values. This is because we employed a fixed value for the return stroke air density (see discussion in section 2g) and because all other cooling mechanisms beyond channel expansion have been neglected (i.e., $L = 0$). Hence, our temperature plots are only valid in representing certain basic features (i.e., the moment of temperature rise, the characteristic

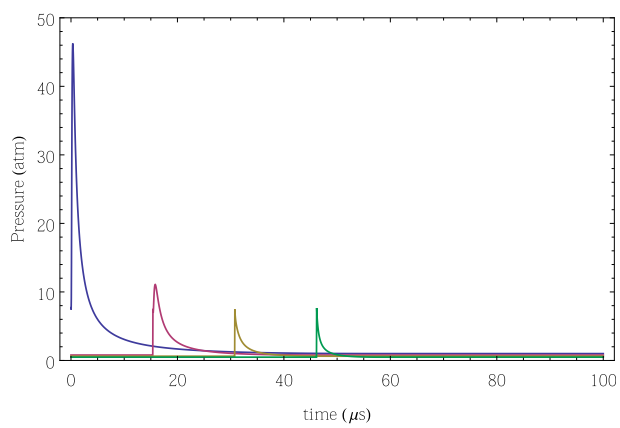

FIG. 6. Channel pressure vs time for various altitudes (model run 1). See Fig. 2 caption for altitude curve color key.

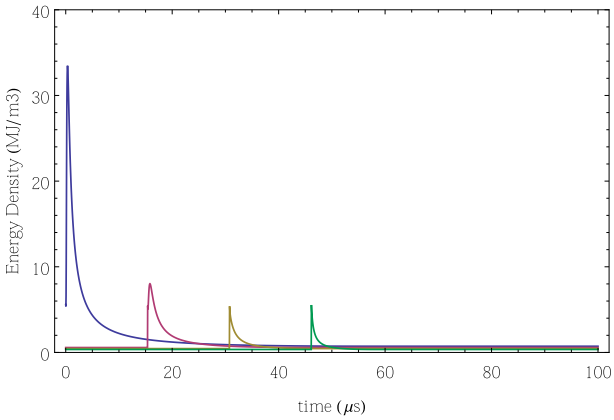

FIG. 7. Channel energy density vs time for various altitudes (model run 1). See Fig. 2 caption for altitude curve color key.

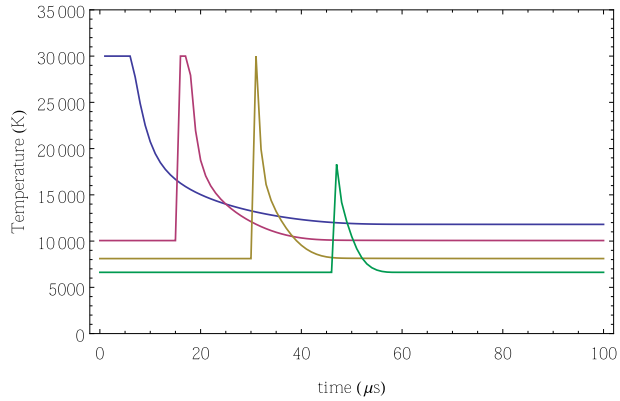

FIG. 8. Channel temperature vs time for various altitudes (model run 1). See Fig. 2 caption for altitude curve color key.

rise time, the characteristic peak temperature if below our artificial cap, and the decay in temperature up to the moment that the constant temperature value is first reached).

Since the amount of model return stroke NO_x depends on the maximum channel radius attained (see section 2h), we expect that our model overestimates NO_x production because of neglect of the ancillary cooling mechanisms mentioned here and the self-magnetic pinch effect, assuming the initial conditions in the boundary value problem are chosen correctly.

b. *Model run 2 (enhanced initial radial velocity)*

In this model run, we employ the same current source as in the baseline run but enhance the initial radial velocity at all altitude levels by a factor of 10 as shown in Fig. 9. This gives the channel radius results shown in Fig. 10. For brevity, we omit the plots of the derived channel variables that have some qualitatively similar attributes to the plots in Figs. 5–8, but of course are of greater amplitude. Note that the maximum channel radii attained in Fig. 10 are larger than those attained in the baseline run of Fig. 4, as expected. However, the effect of a larger initial radial velocity enhances the channel radii more significantly at higher altitudes than at lower altitudes. This is because in the baseline run the highest altitude channel segment had an initial radial velocity of about 0.35 km s^{-1} larger than the lowest channel segment near the ground, but in this model run 2, the highest channel segment has an initial radial velocity about 3.5 km s^{-1} larger than the lowest segment (see Figs. 3 and 9).

c. *Model run 3 (enhanced peak current)*

The peak current at the surface shown in Fig. 2 (blue curve) is just under 11 kA and this defined the baseline run (run 1). For model run 3, we multiply the values of I_{01} and I_{02} given in section 2b by a factor of 10. This results in a peak current at the surface of just under 110 kA as shown in Fig. 11 and represents a large return stroke discharge; that is, only about 5% of negative

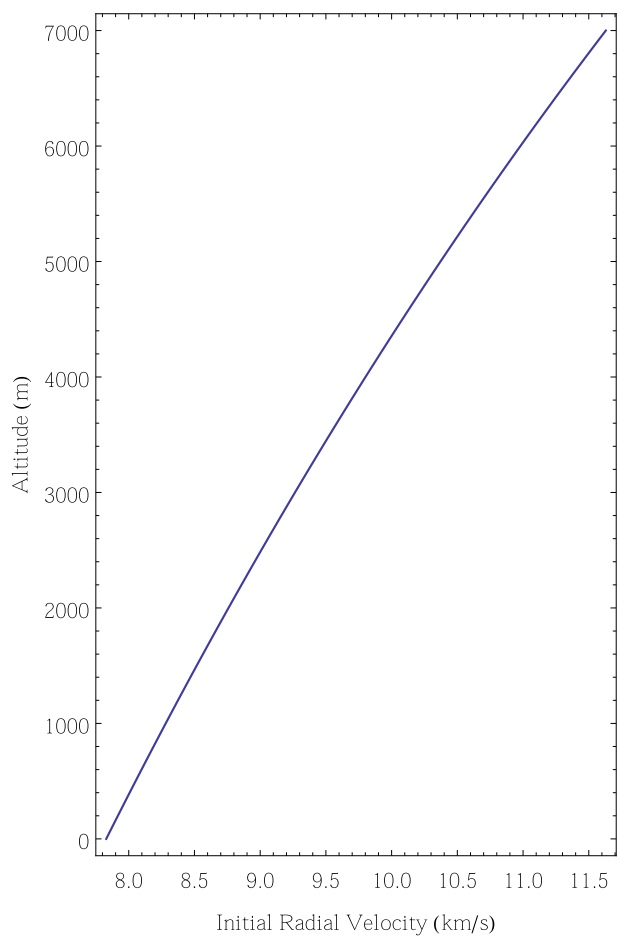

FIG. 9. Initial condition for the channel radial velocity for model run 2.

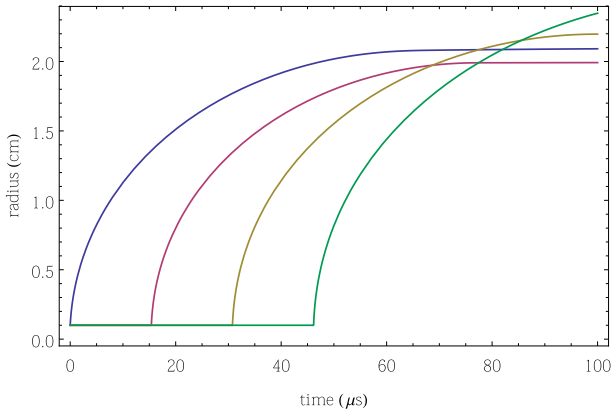

FIG. 10. Channel radius vs time for various altitudes (model run 2). See Fig. 2 caption for altitude curve color key.

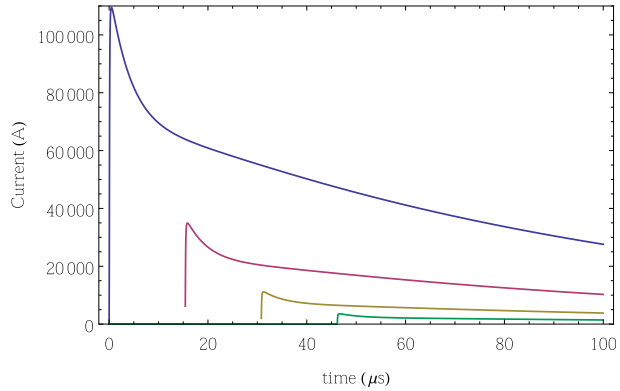

FIG. 11. Current used for model run 3. See Fig. 2 caption for altitude curve color key.

polarity ground flashes have peak currents that exceed 80 kA (Rakov and Uman 2003). Also for this third model run, the initial radial velocity profile is taken as the baseline profile shown in Fig. 3.

Figure 12 shows the channel radius results. Note that the far larger return stroke current leads to more joule heating and hence greater radial expansion. The maximum channel radius at sea level now exceeds 6 cm (i.e., by the time it levels off), which is substantially larger than in either of the previous model runs.

d. *Estimates of total return stroke NO_x*

The altitude profiles for return stroke NO_x production for model runs 1–3 are provided in Fig. 13. The NO_x values are computed for each 1-m-thick vertically oriented cylindrical channel segment using (15), so the vertical resolution in these plots is 1 m. Slight ripples in the curves are produced from the process of extracting the maximum channel radius r_m at each altitude level. After its initial drop, the decay in channel pressure is slow [i.e., p lingers just above $p_e(z)$ for a relatively long time]. Hence, in practice, r_m is obtained by picking the channel radius associated with the channel pressure that first falls within 1013.25 Pa (i.e., 1% of sea level pressure) of the ambient pressure $p_e(z)$. The shape of the profile in Fig. 13b differs from that of the other two profiles because larger maximum channel radii are eventually attained at higher altitudes as shown in the "curve crossovers" in Fig. 10.

These profiles can be used to make estimates of total return stroke NO_x. This involves multiplying an average value of the NO_x per unit channel length by total channel length, as described in greater detail below.

First, it is important to recognize that our model employs an idealized vertical return stroke channel of only 6.5 km, and this is done to simplify the geometry while retaining altitude dependence in the model. Real return stroke channels are tortuous and often highly branched; therefore, the actual total channel length typically extends well beyond the 6.5-km model value. Increases in total channel length increase the total return stroke NO_x.

Therefore, we use the profiles here to obtain an altitude-averaged NO_x density (i.e., the NO_x per unit kilometer of channel in units of moles per kilometer). This average NO_x density is then multiplied by realistic return stroke channel lengths. The average NO_x densities are obtained by summing up the NO_x production from each 1-m-thick channel segment (as obtained from the profile in Fig. 13a, 13b, or 13c) and then dividing by the total channel length of 6.5 km. This gives the following average NO_x densities: 0.045 mol km^{-1} (model run 1, Fig. 13a), 0.265 mol km^{-1} (model run 2, Fig. 13b), and 0.730 mol km^{-1} (model run 3, Fig. 13c).

For an analysis of 4832 flashes from August thunderstorms in Alabama in the years 2005–09, the August average cloud-to-ground lightning channel lengths derived from LNOM were found to range from 38.9 to

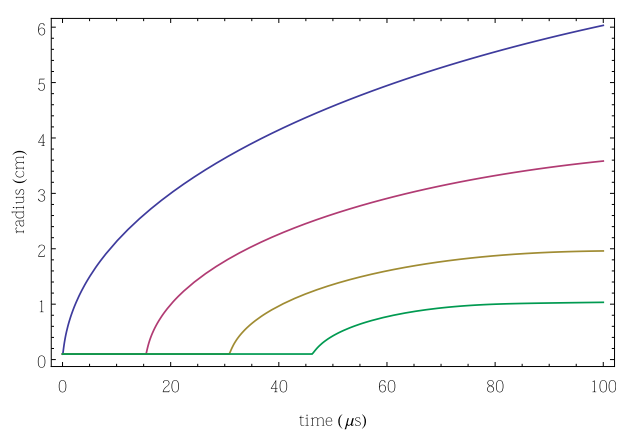

FIG. 12. Channel radius vs time for various altitudes (model run 3). See Fig. 2 caption for altitude curve color key.

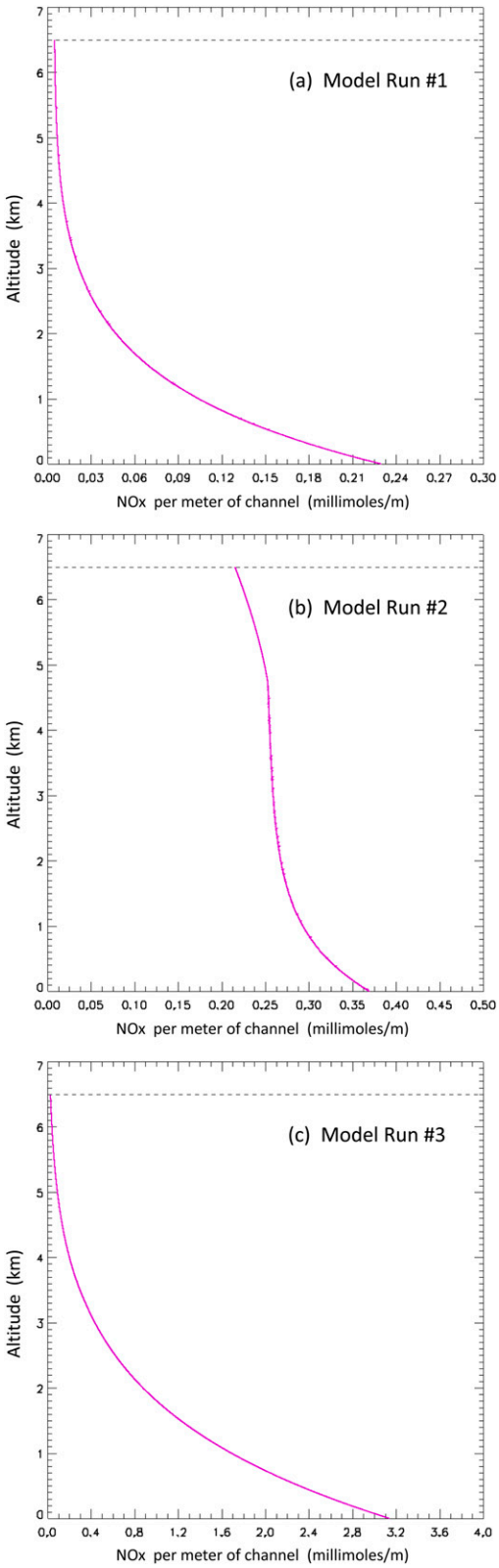

FIG. 13. Return stroke NO_x profiles obtained from the three model runs.

69.6 km (Koshak et al. 2014). These LNOM results are based on a detailed analysis of data from a Lightning Mapping Array (LMA) operating in northern Alabama (Koshak et al. 2004). The present LNOM archive has more extensive statistics and shows an average channel length of 66.9 km for 40 166 cloud-to-ground lightning flashes that occurred across several years and across all months in a year. Using this improved length estimate, and assuming a typical value of three return strokes per ground flash (i.e., a multiplicity of 3), one obtains the following estimates of return stroke NO_x production: 9.0 mol (model run 1), 53.2 mol (model run 2), and 146.5 mol (model run 3). These provide a reasonable range of values that one can obtain depending on just the details of the input parameters to our return stroke model. A larger range of return stroke NO_x estimates can obviously be obtained by including the range of channel lengths and multiplicities that can occur in nature. The average channel length of 66.9 km accounts for channel tortuosity but also all the branches off the main return stroke channel. Since currents are likely smaller in these branches, our NO_x calculations here likely represent an overestimate. In addition, since a subsequent stroke in a ground flash typically has a smaller peak current then the first return stroke (Rakov and Uman 2003), the simple multiplication by the multiplicity, as done above, involves an overestimation.

By comparison, a run of the LNOM for the same 6.5-km model channel and using the baseline peak current value employed in model run 1 gave an average NO_x density of 0.550 mol km^{-1}. This suggests that the LNOM is overestimating the true return stroke NO_x production. One contributing factor to this overestimation is that the LNOM does not attenuate the return stroke current with altitude as given by the $\exp(-z/\lambda)$ factor in (4). Nonetheless, given the large input parameter space associated with our gas dynamic model, we desire future activities devoted to intercomparing model results with LNOM, so that the two can be jointly and optimally tuned. In-depth comparisons and tuning of this nature are beyond the scope of the present work, whose main focus has been to introduce the gas dynamic model. Therefore, the return stroke NO_x values provided above should be considered only as preliminary estimates.

Finally, it is important to emphasize that these NO_x estimates are only for return strokes and do not represent the total NO_x (or so-called LNO_x) produced by a cloud-to-ground flash. There are many other mechanisms that produce additional amounts of NO_x in a cloud-to-ground flash such as continuing currents, *K* changes, *M* components, hot-core stepped and dart leaders, and stepped leader corona sheath (Cooray et al. 2009; Koshak et al. 2014).

4. Summary

A new gas dynamic model has been introduced with the main focus of using it as a tool to estimate NO_x production from return strokes in cloud-to-ground lightning. What distinguishes this model from previous gas dynamic models is that it takes the extra steps required to estimate return stroke NO_x from the model-derived channel properties (i.e., cross-sectional radius, radial expansion rate, pressure, temperature, energy density). To achieve a reasonable estimate of NO_x means that these channel properties had to be solved not only as a function of time but also as a function of altitude. The altitude dependence has essentially been ignored in previous gas dynamic models, but with the aggressive use of 3D Lightning Mapping Array (LMA) data to estimate LNO_x using the NASA LNOM (Koshak et al. 2014), the need for a rigorous analysis of the channel properties across the vertical altitude domain is essential.

Because altitude is included in our model, this allows us to employ a more robust model for the return stroke current source. Whereas previous investigators have used oversimplified current models just at the surface, our model employs a full modified transmission line model across the entire vertical domain of the return stroke channel. Hence, our gas dynamic model includes a realistic vertically propagating current pulse that evolves in altitude and time and is responsible for the joule heating of the channel.

In response to the heating, the cross-sectional channel radius $r(z, t)$ evolves. After generalizing and improving on several important assumptions made by Braginskii (1958), we derived a nonlinear differential equation for $r(z, t)$, where z is viewed as a constant parameter. Employing the latest version of Mathematica available at the time of this study, this differential equation was numerically solved with 0.5-μs time resolution and 1-m spatial resolution. From the values of $r(z, t)$, we extract other channel properties (radial expansion rate, pressure, temperature, and energy density).

Finally, the altitude-dependent maximum channel radii are combined with energy-conservation requirements and results from equilibrium NO_x chemistry findings to make estimates of NO_x production for each meter segment of the return stroke channel; this is described in detail in the derivation of (15) in section 2. Preliminary estimates of total return stroke NO_x were obtained by multiplying our altitude-averaged model NO_x density by LNOM/LMA-derived average ground flash channel length and then multiplying by the expected number of return strokes in a flash. Since we neglect magnetic pinch and all energy loss mechanisms (except cooling due to channel expansion), the results overestimate maximum channel radius and, hence, overestimate LNO_x. In follow-on studies, we intend to retain the magnetic pinch term and may include additional cooling mechanism terms.

Important tunable variables of the model include initial radius and radial expansion of the channel, return stroke current source characteristics (i.e., those parameters defining peak current, rise time, decay time), channel air density, channel conductivity, the temperature-dependent specific heat ratio, and the ambient atmospheric pressure and density profiles. Depending on these input parameters, a fair range of return stroke NO_x estimates can be obtained and compared to empirically based LNOM results. Therefore, we desire more intercomparisons with LNOM return stroke NO_x values in the future to fully optimize and tune both our model and the LNOM.

Acknowledgments. This research has been supported by the NASA Marshall Space Flight Center Science Innovation Fund, under the direction of the MSFC Science and Technology Office Chief Scientist Dr. Melissa Mcgrath. We are grateful to Dr. Mcgrath and Dr. Michael Lapointe of the National Space Science and Technology Center for their helpful guidance and encouragement throughout the term of this effort. In addition, we give special thanks to the manager of the Earth Science Office at MSFC, Dr. James Smoot, for his continued support and guidance during all phases of this work.

REFERENCES

Abramson, I. S., N. M. Gegechkori, S. I. Drabkina, and S. L. Mandel'shtam, 1947: Spark discharge channel. *Zh. Eksperimental'noy Teoreticheskoy Fiz.,* **17,** 863–867.

Archer, C. L., 2004: The Santa Cruz eddy and U.S. wind power. Ph.D. thesis, Stanford University, 190 pp.

Barannik, S. I., S. B. Vasserman, and A. N. Lukin, 1975: Resistance and inductance of a gas arc. *Sov. Phys. Tech. Phys.,* **19,** 1449–1453.

Bauer, E., 1990: Physics of high-temperature air. Part I. Basics. Institute for Defense Analyses D-487, IDA Log HQ 88033544, 125 pp.

Borucki, W. J., and W. L. Chameides, 1984: Lightning: Estimates of the rates of energy dissipation and nitrogen fixation. *Rev. Geophys. Space Phys.,* **22,** 363–372, doi:10.1029/RG022i004p00363.

Braginskii, S. I., 1958: Theory of the development of a spark channel. *J. Exp. Theor. Phys.,* **34,** 1068–1074.

Chameides, W. L., 1986: The role of lightning in the chemistry of the atmosphere. *The Earth's Electrical Environment,* E. P. Krider and R. G. Roble, Eds., National Academies Press, 70–80.

Cooray, V., M. Rahman, and V. Rakov, 2009: On the NO_x production by laboratory electrical discharges and lightning. *J. Atmos. Sol. Terr. Phys.,* **71,** 1877–1889, doi:10.1016/j.jastp.2009.07.009.

DeConti, A., and S. Visacro, 2009: On the use of lumped sources in a nonlinear lightning return stroke model and extension for evaluating strikes to tall objects. *J. Geophys. Res.,* **114,** D11115, doi:10.1029/2008JD011120.

——, ——, N. Theethayi, and V. Cooray, 2008: A comparison of different approaches to simulate a nonlinear channel resistance in lightning return stroke models. *J. Geophys. Res.,* **113,** D14129, doi:10.1029/2007JD009395.

Drabkina, S. I., 1951: On the theory of development of the channel of a spark discharge. *J. Exp. Theor. Phys.,* **21,** 473–483.

Goodman, S. J., and Coauthors, 2013: The GOES-R Geostationary Lightning Mapper (GLM). *Atmos. Res.,* **125–126,** 34–49, doi:10.1016/j.atmosres.2013.01.006.

Heidler, F., 1987: Lightning electromagnetic impulse: Theorie und messungen. Ph.D. thesis, Universität der Bundeswehr, 385 pp.

Hill, R. D., 1987: Comments on "Lightning return stroke. A numerical calculation of the optical radiation." *Phys. Fluids,* **30,** 2585–2586, doi:10.1063/1.866099.

Huntrieser, H., H. Schlager, C. Feigl, and H. Höller, 1998: Transport and production of NO_x in electrified thunderstorms: Survey of previous studies and new observations at midlatitudes. *J. Geophys. Res.,* **103,** 28 247–28 264, doi:10.1029/98JD02353.

Keenan, J. H., J. Chao, and J. Kaye, 1983: *Gas Tables in SI Units*. 2nd ed. John Wiley and Sons, 211 pp.

Koshak, W. J., and E. P. Krider, 1989: Analysis of lightning field changes during active Florida thunderstorms. *J. Geophys. Res.,* **94,** 1165–1186, doi:10.1029/JD094iD01p01165.

——, and H. S. Peterson, 2011: A summary of the NASA Lightning Nitrogen Oxides Model (LNOM) and recent results. *Extended Abstracts, 10th Annual Community Modeling and Analysis System (CMAS) Conf.,* Chapel Hill, NC, EPA/UNC, 6 pp. [Available online at https://www.cmascenter.org/conference/2011/abstracts/koshak_summary_nasa_2011.pdf.]

——, and Coauthors, 2004: North Alabama Lightning Mapping Array (LMA): VHF source retrieval algorithm and error analyses. *J. Atmos. Oceanic Technol.,* **21,** 543–558, doi:10.1175/1520-0426(2004)021<0543:NALMAL>2.0.CO;2.

——, M. N. Khan, A. P. Biazar, M. Newchurch, and R. T. McNider, 2009: A NASA model for improving the lightning NOx emission inventory for CMAQ. *Fourth Conf. on the Meteorological Applications of Lightning Data and 11th Conf. on Atmospheric Chemistry,* Phoenix, AZ, Amer. Meteor. Soc., J8.2. [Available online at https://ams.confex.com/ams/89annual/techprogram/paper_147334.htm.]

——, H. S. Peterson, E. W. McCaul, and A. P. Biazar, 2010: Estimates of the lightning NOx profile in the vicinity of the North Alabama Lightning Mapping Array. *21st Int. Lightning Detection Conf. and Third Int. Lightning Meteorological Conf.,* Orlando, FL, Vaisala Inc., 13 pp. [Available online at http://www.vaisala.com/Vaisala%20Documents/Scientific%20papers/5.Koshak,%20Peterson.pdf.]

——, ——, A. P. Biazar, M. N. Khan, and L. Wang, 2014: The NASA Lightning Nitrogen Oxides Model (LNOM): Application to air quality modeling. *Atmos. Res.,* **135–136,** 363–369, doi:10.1016/j.atmosres.2012.12.015.

Lin, S. C., 1954: Cylindrical shock waves produced by instantaneous energy release. *J. Appl. Phys.,* **25,** 54–57, doi:10.1063/1.1721520.

Nucci, C. A., and F. Rachidi, 1989: Experimental validation of a modification to the transmission line model for LEMP calculations. *Proc. Eighth Symp. on Electromagnetic Compatibility,* Zurich, Switzerland, ETH-Zentrum, 389–394.

——, G. Diendorfer, M. A. Uman, F. Rachidi, M. Ianoz, and C. Mazzetti, 1990: Lightning return stroke current models with specified channel-base current: A review and comparison. *J. Geophys. Res.,* **95,** 20 395–20 408, doi:10.1029/JD095iD12p20395.

Oetzel, G. N., 1968: Computation of the diameter of a lightning return stroke. *J. Geophys. Res.,* **73,** 1889–1896, doi:10.1029/JB073i006p01889.

Orville, R. E., 1968a: A high-speed time-resolved spectroscopic study of the lightning return stroke: Part III. A time-dependent model. *J. Atmos. Sci.,* **25,** 852–856, doi:10.1175/1520-0469(1968)025<0852:AHSTRS>2.0.CO;2.

——, 1968b: Spectrum of the lightning stepped leader. *J. Geophys. Res.,* **73,** 6999–7008, doi:10.1029/JB073i022p06999.

Paxton, A. H., R. L. Gardner, and L. Baker, 1986: Lightning return stroke. A numerical calculation of the optical radiation. *Phys. Fluids,* **29,** 2736–2741, doi:10.1063/1.865514.

——, L. Baker, and R. L. Gardner, 1987: Reply to comments of Hill. *Phys. Fluids,* **30,** 2586–2587, doi:10.1063/1.866100.

Picone, J. M., J. P. Boris, J. R. Greig, M. Raleigh, and R. F. Fernsler, 1981: Convective cooling of lightning channels. *J. Atmos. Sci.,* **38,** 2056–2062, doi:10.1175/1520-0469(1981)038<2056:CCOLC>2.0.CO;2.

Plooster, M. N., 1968: Shock waves from line sources. NCAR Tech. Note NCAR TN-37, 84 pp.

——, 1970: Shock waves from line sources. Numerical solutions and experimental measurements. *Phys. Fluids,* **13,** 2665–2675, doi:10.1063/1.1692848.

——, 1971: Numerical model of the return stroke of the lightning discharge. *Phys. Fluids,* **14,** 2124–2133, doi:10.1063/1.1693303.

Rakov, V. A., and M. A. Uman, 2003: *Lightning: Physics and Effects.* 1st ed. Cambridge University Press, 687 pp.

Sakurai, A., 1954: On the propagation and structure of a blast wave, II. *J. Phys. Soc. Japan,* **9,** 256–266, doi:10.1143/JPSJ.9.256.

Schumann, U., and H. Huntrieser, 2007: The global lightning-induced nitrogen oxides source. *Atmos. Chem. Phys.,* **7,** 3823–3907, doi:10.5194/acp-7-3823-2007.

Stavrakou, T., J.-F. Muller, K.-F. Boersma, R. J. van der A, J. Kurokawa, T. Ohara, and Q. Zhang, 2013: Key chemical NO_x sink uncertainties and how they influence top-down emissions of nitrogen oxides. *Atmos. Chem. Phys. Discuss.,* **13,** 7871–7929, doi:10.5194/acpd-13-7871-2013.

Taylor, G. I., 1950: The formation of a blast wave by a very intense explosion. I. Theoretical discussion. *Proc. Roy. Soc. London,* **201A,** 159–174, doi:10.1098/rspa.1950.0049.

Wang, Y., A. W. DeSilva, G. C. Goldenbaum, and R. R. Dickerson, 1998: Nitric oxide production by simulated lightning: Dependence on current, energy, and pressure. *J. Geophys. Res.,* **103,** 19 149–19 159, doi:10.1029/98JD01356.

Zeldovich, Y. B., and Y. P. Raizer, 2002: *Physics of Shock Waves and High-Temperature Hydrodynamic Phenomena*. Dover Publications, 916 pp.

Zhang, R., X. Tie, and D. W. Bond, 2003: Impacts of anthropogenic and natural NOx sources over the U.S. on tropospheric chemistry. *Proc. Natl. Acad. Sci. USA,* **100,** 1505–1509, doi:10.1073/pnas.252763799.